Journal of Physics B: Atomic, Molecular and Optical Physics

PAPER

Collective effects in photoionization of sodium clusters: plasmon resonance spill, induced attractive force and correlation minimum

To cite this article: Rasheed Shaik *et al* 2021 *J. Phys. B: At. Mol. Opt. Phys.* **54** 125101

IOP Publishing Journal of Physics B: Atomic, Molecular and Optical Physics
J. Phys. B: At. Mol. Opt. Phys. **54** (2021) 125101 (10pp) https://doi.org/10.1088/1361-6455/ac03c9

Collective effects in photoionization of sodium clusters: plasmon resonance spill, induced attractive force and correlation minimum

Rasheed Shaik[1], **Hari R Varma**[1,*] **and Himadri S Chakraborty**[2,*]

[1] School of Basic Sciences, Indian Institute of Technology Mandi, Kamand, H.P. 175075, India
[2] Department of Natural Sciences, D.L. Hubbard Center for Innovation and Entrepreneurship, Northwest Missouri State University, Maryville, Missouri 64468, United States of America

E-mail: hari@iitmandi.ac.in and himadri@nwmissouri.edu

Received 19 February 2021, revised 14 May 2021
Accepted for publication 21 May 2021
Published 11 June 2021

Abstract

Photoionization studies of Na_{20} and Na_{92} clusters are carried out in a framework of linear response density functional theory. Cross sections show substantial spillover of plasmon resonances to the near-threshold ionization energies which are in reasonable agreements with photoabsorption measurements. The analysis of the oscillator strength, consumed by the cross section, lends further detailed insights. The many-body interaction induced self-consistent field from density fluctuations suggests the existence of an attractive force. This may cause time-delayed plasmonic photoemissions in ultrafast measurements. At the waning end of the plasmon structure, a strong minimum in the cross sections from a correlation-driven coherence effect is predicted which can possibly be observed by the photoelectron spectroscopy.

Keywords: collective effects in photoionization, sodium clusters, plasmon resonances, correlation minimum

(Some figures may appear in colour only in the online journal)

1. Introduction

The physics of atomic clusters has gained broad importance as a domain of study of new physical objects, often termed as super-atoms, over the past few decades [1]. Such clusters are aggregates of atoms, ranging from two to a few thousand of atoms, and provide the platform to study a new phase of matter intermediate to atoms or molecules and solids [2]. These systems also offer valuable opportunities to understand how the bulk properties emerge from their individual constituent atoms [3]. Possibilities of designing new class of materials with tailor made characteristics using clusters as building blocks, instead of atoms, have rendered this field diverse and vibrant [4]. The extensive research on clusters over the years has revealed many unusual properties which are of interests to the field of physical and chemical sciences, material sciences, and biological sciences, making these explorations interdisciplinary in nature [5].

Many intriguing phenomena are associated with the photoresponse spectrum of atomic clusters [6]. These include phenomena, such as, plasmon resonances [7–9], fano type resonances [10], and diffractive modulations [11] in the photoelectron signal due to the largely well-defined cluster edges [12]. One primary focus of the present work is the photoionizing response of the plasmon resonances—resonances that form due to the collective oscillations of the valence electron cloud. Excitation of a lower energy giant surface plasmon resonance is known to be a prominent feature in the photoresponse of neutral alkali metal clusters that occurs below the ionization threshold energy. On the other hand, for anion clusters this resonance appears in the continuum (ionization) energy region [13]. Giant resonances in metal clusters have

* Authors to whom any correspondence should be addressed.

applications in nano-optical devices, chemical and biological sensing, and bio-medicine etc [14–16], besides their eminent role as 'spectral laboratories' to assess many-electron effects. Therefore, developing detailed and accurate understanding of the origin, the underlying dynamics, and related observable effects of this resonance are a matter of significant priority.

In addition, the presence of a higher-energy volume like plasmon makes the photo-spectrum of atomic clusters [7] more robust compared to the spectrum of the corresponding bulk metal. It is well known that due to the translational invariance, the coupling of the volume oscillation in bulk to light is not feasible [17]. However, the situation is different for the case of finite systems like metal clusters due to the broken translational invariance that may cause boundary reflections of the plasma wave. As a result, optically active volume plasmon resonance can also become possible. The presence of such a volume plasmon excitation is observed for the first time in the experimental work of Xia *et al* [7]. Their photon depletion measurements of Na_{20} and Na_{92} clusters showed a broad volume plasmon resonance mounted on the decay ridge of giant surface plasmon and peaking slightly above 4 eV. The tail of this combined structure was found extended to the ionization region. The present calculation is motivated to address this spillover part of the plasmon structure closely above the ionization threshold. In studying this, we also predict a universal minimum at the decay end of the structure from an interchannel coupled phase-coherence effect arising from many-electron correlations. Furthermore, an analysis of the many-body induced self-consistent field potential at the plasmon spillover energies point to a correlation driven attractive force that suggests possible time delays of the emerging photoelectron.

The dynamical response of the Na clusters to the external electromagnetic radiation is calculated using a linear response density functional theory (DFT) approach. A fairly competent method belonging to this class is the jellium based time-dependent local density approximation (TDLDA) [18]. In the past, application of TDLDA to atomic clusters is found to be successful in explaining the collective phenomena occurring at low energies [8] and also the diffractive oscillations present at high energies [12]. The ease and transparency of a jellium based model enable physicists to interpret the key physics that determines the dynamics. A recent study on fullerenes indicated that a better agreement with experiment can be obtained by using one such DFT approach with Leeuwen–Baerends (LB94) exchange–correlation (xc) functional that produces the correct ground state asymptotic properties [19]. Another study has tested the efficacy of the method for Na clusters [20]. Hence, this method is chosen in the present work.

The paper is organized in the following way. A basic description of the theoretical methodology is provided in section 2 which has two parts. The details of ground state structure in the spherical jellium formalism along with a brief account of the LB94 parameterization scheme is provided in section 2.1. A brief description of the method that incorporates electron correlations in response to the radiation is given in section 2.2. Section 3 constitutes the results and discussions of: photoionization cross sections and its comparison with experiment (section 3.1), the photoelectron oscillator strength (OS) (section 3.2), the many-body correlation induced potential in the spillover region of plasmon (section 3.3), and the prediction of a 'correlation minimum' at the high-energy end of the plasmon structure (section 3.4). Finally, section 4 concludes the study. Results are shown in atomic units (a.u.), unless indicated otherwise.

2. Theoretical methodology

2.1. *Ground states of* Na_{20} *and* Na_{92}

To investigate the ground state electronic structure of Na_N ($N = 20$ and 92), a DFT approach is adopted. For such systems of closed-shell configurations the jellium model serves as a very good approximation. In this model, the jellium potential ($V_{\rm jel}(r)$) replaces the ionic core of 20 and 92 Na^+ ions, respectively for Na_{20} and Na_{92}, by potentials constructed after homogeneously smearing their positive charges into jellium spheres. The potential $V_{\rm jel}(r)$ is generated by the distribution:

$$V_{\rm jel}(r) = \begin{cases} -\dfrac{N}{2R_{\rm c}}\left(3 - \left(\dfrac{r}{R_{\rm c}}\right)^2\right), & r \leqslant R_{\rm c} \\ -\dfrac{N}{r}, & r > R_{\rm c} \end{cases}.$$

The radius of each cluster is determined by the number N of ions present in the system. The radius of Na_{20} is calculated to be 10.67 a.u. and that of Na_{92} to be 17.74 a.u. using the formula $R_{\rm c} = r_{\rm s}N^{1/3}$, where $r_{\rm s}$ is the Wigner–Seitz radius (3.93 a.u.) of a Na atom. The Kohn–Sham equations for N delocalized valence electrons, the $3s^1$ electron from each Na atom, are solved to obtain the ground state structures of Na_{20} and Na_{92}. It is to be noted that to match the valence ionization thresholds with the experimental values [21], suitable constant pseudo potentials are added.

In terms of the single-particle density $\rho(\boldsymbol{r})$, the ground state self-consistent field LDA potential reads as,

$$V_{\rm LDA}(\mathbf{r}) = V_{\rm jel}(r) + \int {\rm d}\mathbf{r}' \frac{\rho(\mathbf{r}')}{|\mathbf{r} - \mathbf{r}'|} + V_{\rm xc}[\rho(\mathbf{r})], \qquad (1)$$

where the second and third terms on the rhs are respectively the direct and xc potentials. Approximate form for $V_{\rm xc}$ has to be used since its exact form is unknown. In the present work, we approximate the $V_{\rm xc}$ with the LB94 functional which provides an accurate asymptotic description of the ground-state properties. This functional belongs to a gradient corrected class of approximation by van Leeuwen and Baerends, parameterized in terms of the reduced density and its gradient $\nabla\rho(\boldsymbol{r})$ [22], to be given by,

$$V_{\rm LB} = -\beta[\rho(\mathbf{r})]^{1/3}\frac{(\xi X)^2}{1 + 3\beta\xi X \sinh^{-1}(\xi X)}, \qquad (2)$$

where $\beta = 0.01$ is a fitting parameter and $X = [\nabla\rho]/\rho^{4/3}$. The parameter ξ arises due to the change of system from

Table 1. Binding energies (BE) of HOMO and HOMO-1 levels of Na_{20} and Na_{92} in the harmonic oscillator notation.

	BE_{HOMO} (eV)	BE_{HOMO-1} (eV)
Na_{20}	$2s - 3.75$	$1d - 4.20$
Na_{92}	$1h - 3.47$	$3s - 3.57$

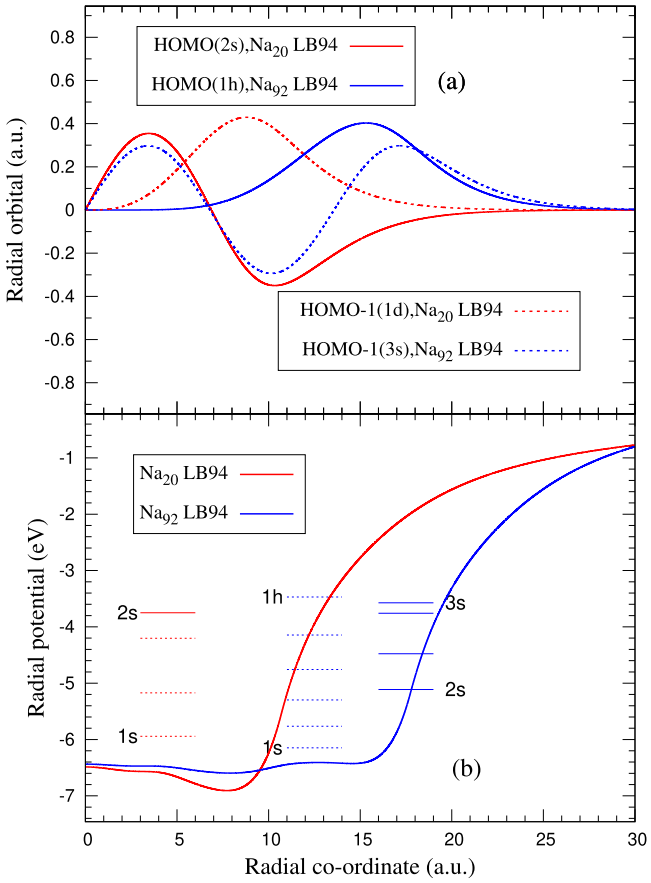

Figure 1. (a) Ground-state radial wavefunctions for HOMO and HOMO-1 levels calculated for Na_{20} and Na_{92}. (b) Ground-state radial potentials and energy levels calculated for Na_{20} and Na_{92}.

spin-polarized to spin-unpolarized form [23]. This scheme of gradient correction of density is derived from a gradient expansion series that naturally eliminates self-interactions and produces the correct asymptotic behavior.

The calculated binding energies of the highest occupied molecular orbitals (HOMO) and (HOMO-1) of these systems, of 2s and 1d character respectively for Na_{20} and 1h and 3s respectively for Na_{92}, are given in table 1 and their radial wavefunctions are shown in figure 1(a). It can be seen that HOMO level of Na_{20} has a single node whereas Na_{92} is nodeless. The situation reverses for HOMO-1. As a result, the radial structures of HOMO and HOMO-1 wavefunctions significantly differ in these two systems. Figure 1(b) shows the ground-state radial potentials of Na_{20} and Na_{92} clusters and the level energies.

2.2. Dynamical response

The dynamical response of the cluster subjected to the external dipole field 'z' can be calculated by employing a linear-response DFT scheme, known as time-dependent LDA (TDLDA) modified by LB94 [24]. The dipole field can induce a frequency-dependent complex change in the electron density $\delta\rho$ [25], which, within a linear-response perturbative framework, can be written as:

$$\delta\rho(\mathbf{r}';\omega) = \int \chi(\mathbf{r},\mathbf{r}';\omega) z \mathrm{d}\mathbf{r}, \tag{3}$$

where χ is the full susceptibility of the system which incorporates all the dynamical electron correlations. The above equation can be re-written in terms of independent particle (IP) susceptibility, χ_0, and the complex field δV as,

$$\delta\rho(\mathbf{r}';\omega) = \int \chi_0(\mathbf{r},\mathbf{r}';\omega)\delta V(\mathbf{r};\omega)\mathrm{d}\mathbf{r}, \tag{4}$$

where χ_0 is constructed by the ground-state single-electron orbitals ϕ_{nl} and energies ϵ_{nl} [26]. The IP susceptibility χ_0 is related to χ by the matrix equation:

$$\chi = \chi_0[1 - (\partial V/\partial\rho)\chi_0]^{-1}. \tag{5}$$

The total field, δV, is given by the following relation:

$$\delta V(\mathbf{r};\omega) = z + V_{\mathrm{ind}}(\mathbf{r};\omega), \tag{6}$$

where

$$V_{\mathrm{ind}}(\mathbf{r};\omega) = \int \frac{\delta\rho(\mathbf{r}';\omega)}{|\mathbf{r}-\mathbf{r}'|}\mathrm{d}\mathbf{r}' + \left[\frac{\partial V_{\mathrm{XC}}}{\partial\rho}\right]_{\rho=\rho_0} \delta\rho(\mathbf{r};\omega). \tag{7}$$

Using the matrix inversion method [27], equation (5) is finally solved for χ which in turn is used for obtaining $\delta\rho$ and thereby δV by making use of equations (3) and (6) in a self-consistent way.

In this formalism, the photoionization cross section corresponding to a bound-to-continuum dipole transition $n\ell \to k\ell'$ is then calculated using

$$\sigma_{n\ell\to k\ell'} \sim |\langle k\ell'|\delta V|n\ell\rangle|^2. \tag{8}$$

It is clear from the above equation that in addition to the external perturbation z, the calculation involves the complex induced field V_{ind} driven by the many-electron correlations. Obviously, setting $\delta V = z$ yields the IP LDA cross section that ignores correlations. A comparison of LDA and TDLDA, therefore, easily possible in this method to study the role of many-electron effects in the photoionization process.

3. Results and discussion

3.1. Photoionization cross-sections and comparison with measurements

Total photoionization cross-section of Na_{20} and Na_{92} clusters, calculated in TDLDA + LB94 and the corresponding

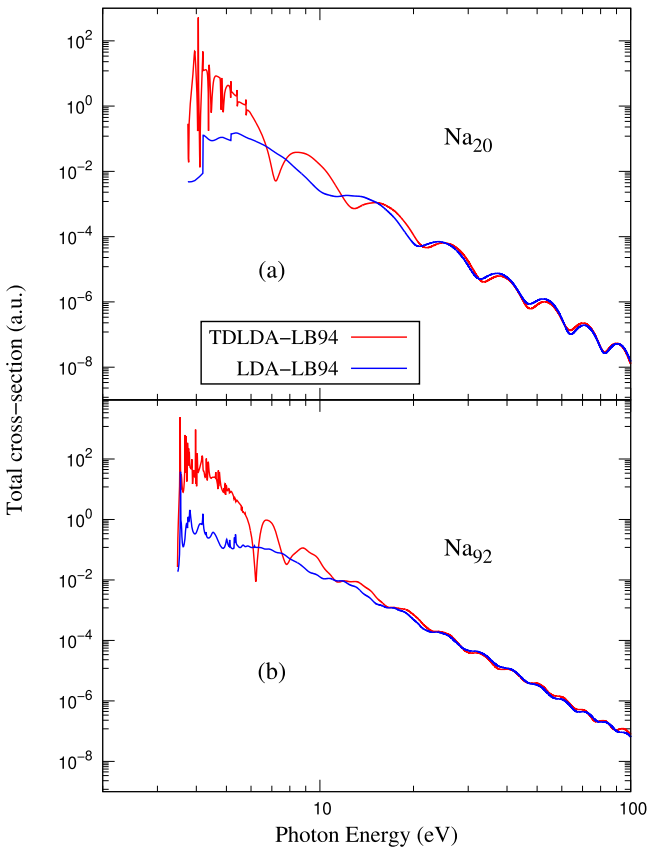

Figure 2. TDLDA and LDA cross sections of Na_{20} (a) and Na_{92} (b).

LDA results, are shown in figures 2(a) and (b) respectively. As seen, the TDLDA cross section profiles, as a function of photon energies, strongly differ from the LDA profiles by (i) significant enhancements near the ionization threshold region, (ii) the presence of autoionization resonances, and (iii) the appearance of a minimum at about 7.20 eV for Na_{20} and 6.22 eV for Na_{92}. The near-threshold enhancement in TDLDA cross sections combines the remnant of the giant surface plasmon resonance, that flourishes below the ionization threshold, and a major portion of the broader volume plasmon resonance, both emerging from the collective electronic motions when subjected to an external electromagnetic field. This resonance spillover from the discrete to continuum spectrum is embedded by a host of narrow spikes, which are the autoionization resonances resulting from the degeneracy of ionization channel with the inner-level single-electron discrete excitations.

In the perturbative interchannel coupling frame of Fano [28], the TDLDA matrix element $M_{n\ell\to k\lambda}(E)$ of a dipole ionization channel $n\ell \to k\lambda$ can be represented as [24]

$$M_{n\ell\to k\lambda}(E) = D_{n\ell\to k\lambda}(E) + \sum_{n'\ell'\neq n\ell}\int dE' \times \frac{\langle\psi_{n'\ell'\to k'\lambda'}(E')|\frac{1}{|\mathbf{r}_{n\ell}-\mathbf{r}_{n'\ell'}|}|\psi_{n\ell\to k\lambda}(E)\rangle}{E-E'} \times D_{n'\ell'\to k'\lambda'}(E'), \quad (9)$$

where $D_{n\ell\to k\lambda}$ is the unperturbed (LDA) matrix element, $|\psi\rangle$ refer to interacting continuum *channel* wavefunctions and the sum runs over all degenerate continuum channels that couple, except the $n\ell$ channel. The matrix element within the integral of equation (9) is known as the interchannel coupling matrix element. The second term in equation (9) embodies important electron correlations that build the strength of the plasmon resonance spill in the $n\ell \to k\lambda$ channel from an in-phase coherence mechanism discussed elsewhere [24]. Equations similar to equation (9) for other channels justify similar enhancements at the same energies for all the subshells [figure 6] of a cluster at the spillover energy region. Consequently, the sum over all subshells adds up *coherently*, leading to the dramatic enhancement of the TDLDA cross section [figure 2]. But, as seen in figures 2 and 3, no enhancement is seen in the LDA predictions which neglect the electron correlations. Structures in the LDA profiles in this near-threshold region are due to the gradual openings of inner-level ionization channels. However, the interpretation of narrow resonances in the Fano frame needs bound-continuum channel coupling, for which the coupling matrix element in equation (9) will modify as [29],

$$\langle\psi_{n'\ell'\to\eta'\lambda'}|\frac{1}{|\mathbf{r}_{n\ell}-\mathbf{r}_{n'\ell'}|}|\psi_{n\ell\to k\lambda}\rangle,$$

where $n'\ell' \to \eta'\lambda'$ denote discrete excitation channels. The jellium-based delocalized wavefunctions [figure 1(a)] are diffused that spread over too large a distance. Hence, the above coupling matrix element of $\frac{1}{\mathbf{r}_{n\ell}-\mathbf{r}_{n'\ell'}}$ involving such spread out wavefunctions translates to a small value. Consequently, the TDLDA model predicts small autoionization rates, producing widths that may be overtly narrow. Such narrow autoionization resonances in jellium-based TDLDA calculations of clusters are not uncommon. They were predicted in photoionization studies of fullerenes [19] and in inter-Coulombic decay (ICD) resonances in endofullerenes [30]. However, it is difficult to confirm, in the absence of experiments, how unrealistic the predicted widths are. As a fundamental effect, electron delocalization being an intrinsic character of clusters will likely produce narrower autoionization resonances than those in atoms in which wavefunctions are highly localized.

The existence of the volume plasmon resonance and the extended tail of the surface resonance to the ionization part is experimentally seen in the work of [7]. Comparisons of our photoionization calculations with these measured photoabsorption data is shown in figure 3(a) for Na_{20} and figure 3(b) for Na_{92}. For this comparison, the theoretical total cross section per atom is evaluated for each cluster and an appropriate unit conversion is carried out, from a.u. to $\mathring{A}^2$, by multiplying with a_0^2 where $a_0 = 0.529\ \mathring{A}$ is the Bohr radius. The data covers the range of 2 eV to 5.64 eV. Following reference [7], fits to the experimental data as a sum of four Lorentzian profiles for Na_{20} and a sum of three for Na_{92} are also shown in figure 3. It is to be noted that fitting is done not to smear out the narrow autoionization resonances but to fit only the background plasmon structure. The lower energy Lorentzians in both cases represent the giant portion of the plasmon below

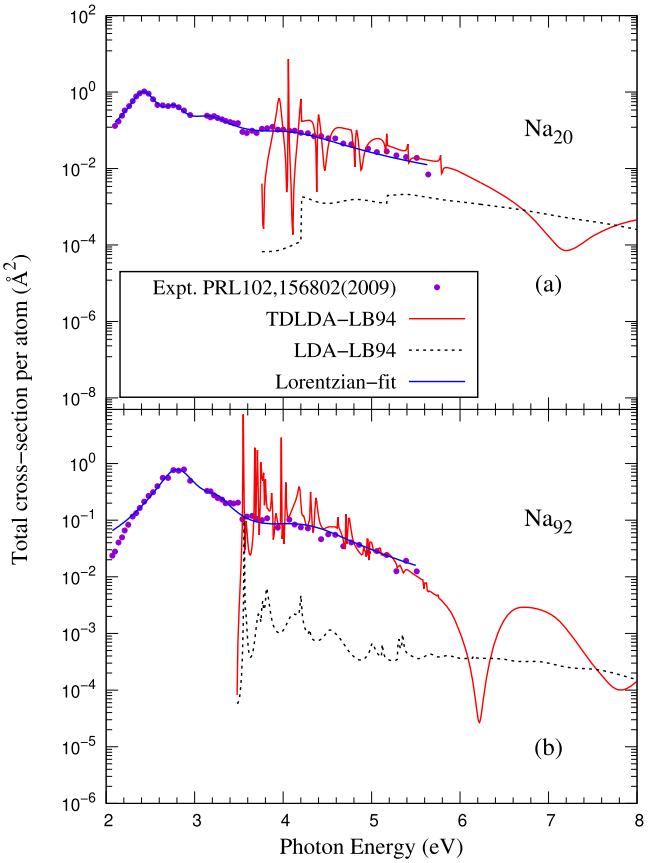

Figure 3. TDLDA cross sections along with experimental data from [7] for Na_{20} (a) and Na_{92} (b). Lorentzian fits to the experimental cross sections are also shown. LDA results are added for comparisons.

Table 2. Resonance positions (E_o), FWHM (Γ) of the higher energy plasmon (HEP) [7].

	E_o (eV)	Γ (eV)
Na_{20} HEP	4.04	1.19
Na_{92} HEP	4.20	1.16

the first ionization threshold that our photoionization results cannot access. The present TDLDA calculations span the ionization part of the spectrum only and, as noted, overlap very well with the higher energy Lorentzian fits used for both the clusters. The peak energy position (E_0) and width (Γ) of the fourth Lorentzian curve for the higher energy plasmon resonance (HEP) for Na_{20} and the corresponding position and width for the third Lorentzian curve for Na_{92} are shown in table 2. It is clear from the figure that the steady background parts of TDLDA cross sections agree well with the experiment describing the spillover of the plasmon resonances. As the size of the cluster increases the peak positions of the volume plasmon shifts to higher energies (blue shifted). Curiously, this size effect is found to be opposite in the case of fullerenes (C_{60} and C_{240}) where peak positions shifted to lower energies as the size increased [19].

It is to be noted that the narrow autoionization resonances are missing in the experimental data. This is likely due to the finite temperature effects of the metal clusters in experimental conditions. This lead to the coupling of electronic motion with the temperature induced vibrational and rotational modes [31] and fluctuation of the cluster shape around the shape of absolute zero temperature [32]. The narrow widths of these resonances may enable their intrinsic time scale longer and comparable with these 'molecular' motions to facilitate the coupling. This was also found and discussed earlier for C_{60} for which photoelectron intensity measurements showed rather smooth profile [24]. One standard way to approximately invoke temperature effects in the numerical calculations is by including a width [8, 24]. But that next step will be appropriate when direct photoionization measurements are available for neutral clusters.

Recent angle-resolved photoelectron spectroscopy (PES) measurements of angular distribution anisotropy parameter β of Na_n^- cluster anions [13] were found free from autoionization resonances even after being carried out at low temperature of 6 K. Subsequent results using RPAE with jellium model also did not reveal narrow resonances [33, 34]. The absence of such structures in these works could be due to the reduction of excited states degenerate with plasmonic ionization in anions compared to neutrals. It may also be due to the fact that the β parameter involving ratios of emission amplitudes weakens the resonance effects from some cancellation. All these, however, points to the need for photoionization measurements of neutral clusters, especially given the overall agreement of our background TDLDA cross section with the absorption data, as seen in figure 3.

3.2. Oscillator strength

From the experimental data shown in figure 3, it is quite clear that the bulk of the absorption OS is consumed in the excitation part of the spectrum below the ionization threshold. In order to get a quantitative measure of the fraction of the OS exhausted in the ionization process, we introduce an 'accumulative' OS as a function of photon energy given by the following relation:

$$OS_t(E_f) = OS_b + \int_{E_{th}}^{E_f} \sigma(E)\mathrm{d}E, \qquad (10)$$

where OS_b is defined as the baseline OS that is calculated by integrating the experimental cross section [7] from the starting photon energy of the measurement to the theoretical ionization thresholds (E_{th}). OS_b therefore corresponds to the OS exhausted by the plasmon resonances below the threshold. The second term in equation (10) corresponds to the incremental addition to the OS_b, cumulatively with energy, due to the plasmon spill to the ionization region from E_{th} to E_f. Here E_f will vary from E_{th} onwards allowing us to calculate OS_t as a function of E_f. Note that until 5.64 eV, the photon energy corresponding to the last experimental datum, E_f's are the various energies for which experimental measurements are available. In equation (10), $\sigma(E)$ corresponds to TDLDA total cross section for the calculations of theoretical OS_t. For calculating the experimental OS_t, on the other hand, $\sigma(E)$ corresponding to

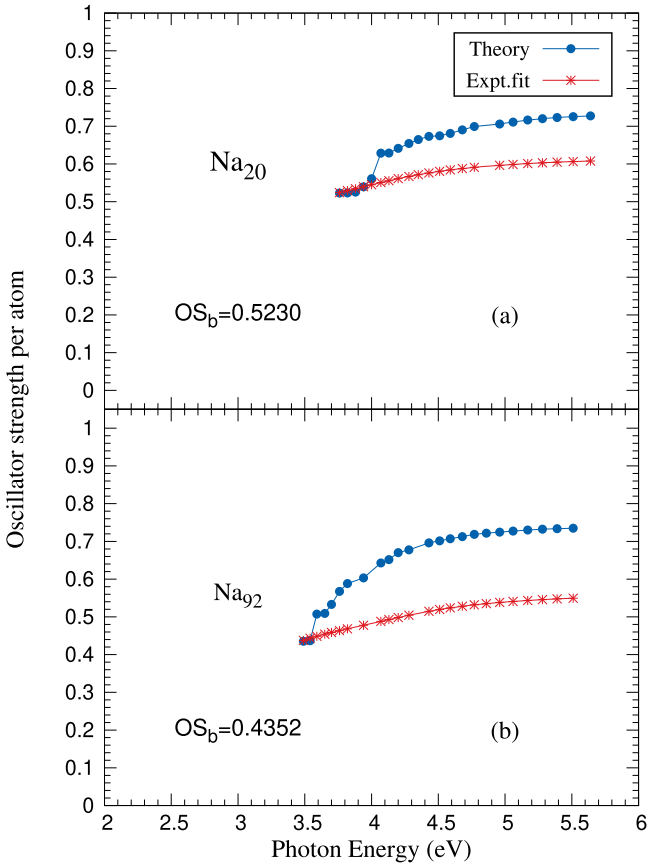

Figure 4. Accumulative oscillator strengths for Na_{20} (a) and Na_{92} (b) where the theoretical results are calculated using the present TDLDA + LB94 cross sections and the experimental OS are calculated using fitted values to the data in [7].

fitted cross section data between two successive measurements [7] are used.

Figure 4 shows OS on a zero-to-one scale, because it represents OS per atom, that is the total OS divided by N. For Na_{20}, the $OS_b = 0.5230$ and for Na_{92}, $OS_b = 0.4352$. These suggest that about 52% of OS is exhausted below the ionization threshold of Na_{20}, while it is about 44% for Na_{92}. The implication is that more fraction of electrons are available to participate in the ionization process for the larger cluster. Hence, the size of plasmon spill increases for Na_{92}. The rise of the theoretical OS curve above the experimental curve is due primarily to the narrow autoionization resonances in the theoretical spectrum which add strengths. This accounts roughly about 20% of OS for Na_{20}, while it is 30% for Na_{92}. As discussed earlier, the experimental measurements cannot likely access these narrow single particle resonances due to the finite temperature effects. However, the corresponding OSs cannot be lost and may transfer to different photon energies.

One comment should be made about the measurements though. The energy deposited into the cluster will not only dissipate through ionization that we calculate, but also be shared with thermalization and evaporation channels as well. Even though the corresponding branching ratio is unknown, we note the following: (i) the direct ionization, that provides the smooth background contribution of the TDLDA results, is known to be a much faster process (in attoseconds) for clusters [35, 36]. (ii) In contrast, the thermalization/evaporation processes, that include ionic vibration, take far longer times (in femtoseconds) [37, 38]. Therefore, it is conceivable that the dominant contribution to the measured absorption data above the ionization threshold energy is from the ionization process—the process that can quickly utilize the energy absorbed. This may not be true below the threshold where the excited electron can decay to thermalize. Of course, a more detailed calculation including electron–phonon coupling, which is beyond the scope of the current study, is necessary to validate our speculation. For now, it is interesting to note that even without that coupling, the present calculation show good agreement with the overall background plasmon spill in absorption measurements. However, the remaining uncertainties underlines the need for direct photoionization measurements of clusters to acquire detailed insights.

3.3. Collectivity induced field

TDLDA dipole matrix element $\langle k\ell'|z + V_{\rm ind}|n\ell\rangle$ in equation (8) requires knowledge of $V_{\rm ind}$, which is the complex induced field driven by electron correlations and is singularly responsible for the plasmonic enhancement in the cross section. The behavior of the real and imaginary parts of $V_{\rm ind}$ across the collective resonance region is well known [39, 40]. $\mathrm{Im}(V_{\rm ind})$ characteristically shows a well-type shape across the energy range of the resonance where the minimum of the well occurs near the energy of the resonance peak. On the other hand, $\mathrm{Re}(V_{\rm ind})$ executes an oscillation by switching the sign over this range where it sluices through the zero at the resonance peak. These two distinct behaviors can be combined in a unified picture. $\mathrm{Im}(V_{\rm ind})$ has a predominant collective character, while $\mathrm{Re}(V_{\rm ind})$ represents effects of the external field. Therefore, as the resonance builds with increasing energy and approaches its peak, the effect of external field reduces [$\mathrm{Re}(V_{\rm ind}) < 0$, the screening] while the collective motion grows. At the peak, the effect of external field is negligible [$\mathrm{Re}(V_{\rm ind}) \sim 0$], where the collective response dominates. At the decaying part of the resonance this trend reverses [$\mathrm{Re}(V_{\rm ind}) > 0$, the antiscreening].

In the current study, however, we access the remnant of the plasmon structure spilling over to the photoionization channel which is fragmented by many single electron narrower resonances mixing coherently with the plasmon effect. This coherence indicates that there are interferences between the single electron Auger process and collective plasmon. So the simple mechanism expressed above becomes complex, the induced field becomes structured, but an interesting general trend should remain that we now explain.

Figure 5 shows the 3D plots of real and imaginary part of radial induced field, $V_{\rm ind}(r;\omega)$, for Na_{20} and Na_{92}. All the plots show many smaller structures, which are because of single-electron resonances that become relatively stronger as the plasmon spill gradually weakens with increasing energy. However, notice the broad shapes in $\mathrm{Im}(V_{\rm ind})$ for both systems. Each shape appears like the ridge of a full-size well whose

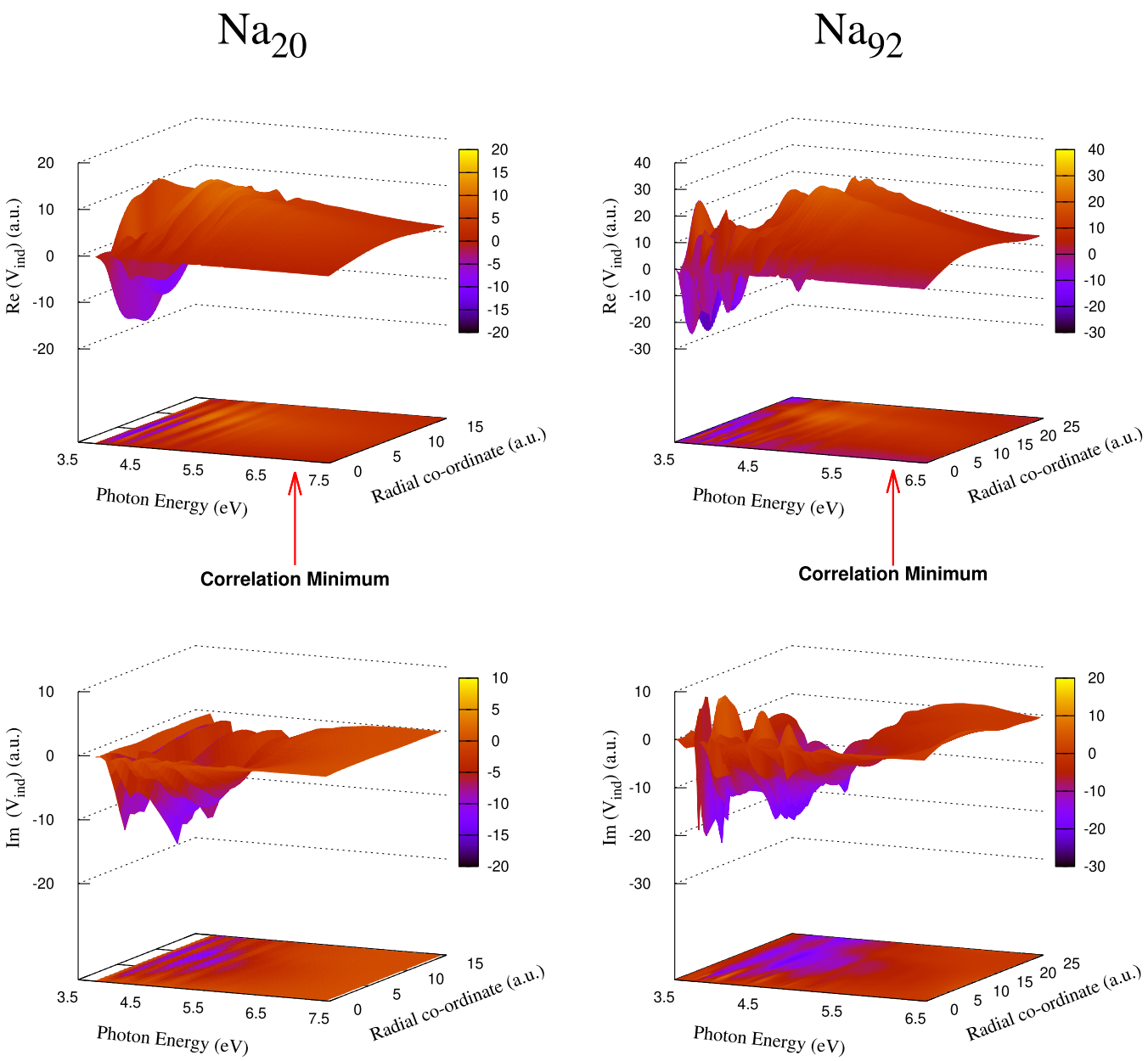

Figure 5. The real and imaginary part of radial self-consistent field potential, $V_{\rm ind}(r)$, for Na_{20} (left panels) and Na_{92} (right panels). Some smoothening is implemented for visual aid. Small arrows pointing on the energy axis in the Re($V_{\rm ind}$) panels indicate the energies of correlation minima.

bottom must be below the ionization threshold where the plasmon structure actually peaks. The shapes suggest the emergence of transient attractive fields as a result of the electrons' collective dynamics. Consequently, the liberating photoelectrons will experience a resistance against their exit and will likely slow down. This can lead to observable time-delayed emissions of electrons [41] in the plasmon spillover range. Particularly, this may find relevance in the context of the electron's intrinsic Wigner-type delay properties [42]. Time delay studies in photoemission belong to a contemporary field of interest based on methods of attosecond photoemission measurements in RABITT or streaking spectrometry [43]. Similar attractive force, driven by electronic collective interactions, has earlier been predicted at plasmon photoionization energies of C_{60} [44].

A remark on the shape of Re($V_{\rm ind}$) may also be in order. Barring the finer structures from single electron resonances, the overall shapes of Re($V_{\rm ind}$) for both systems emerge like incomplete domes. These shapes are expected and clearly suggest the antiscreening behavior, Re($V_{\rm ind}$) > 0, as characteristic of the plasmon decay.

3.4. Correlation minimum

As seen in figure 2, the total photoionization cross sections undergo oscillations both in LDA and TDLDA starting from

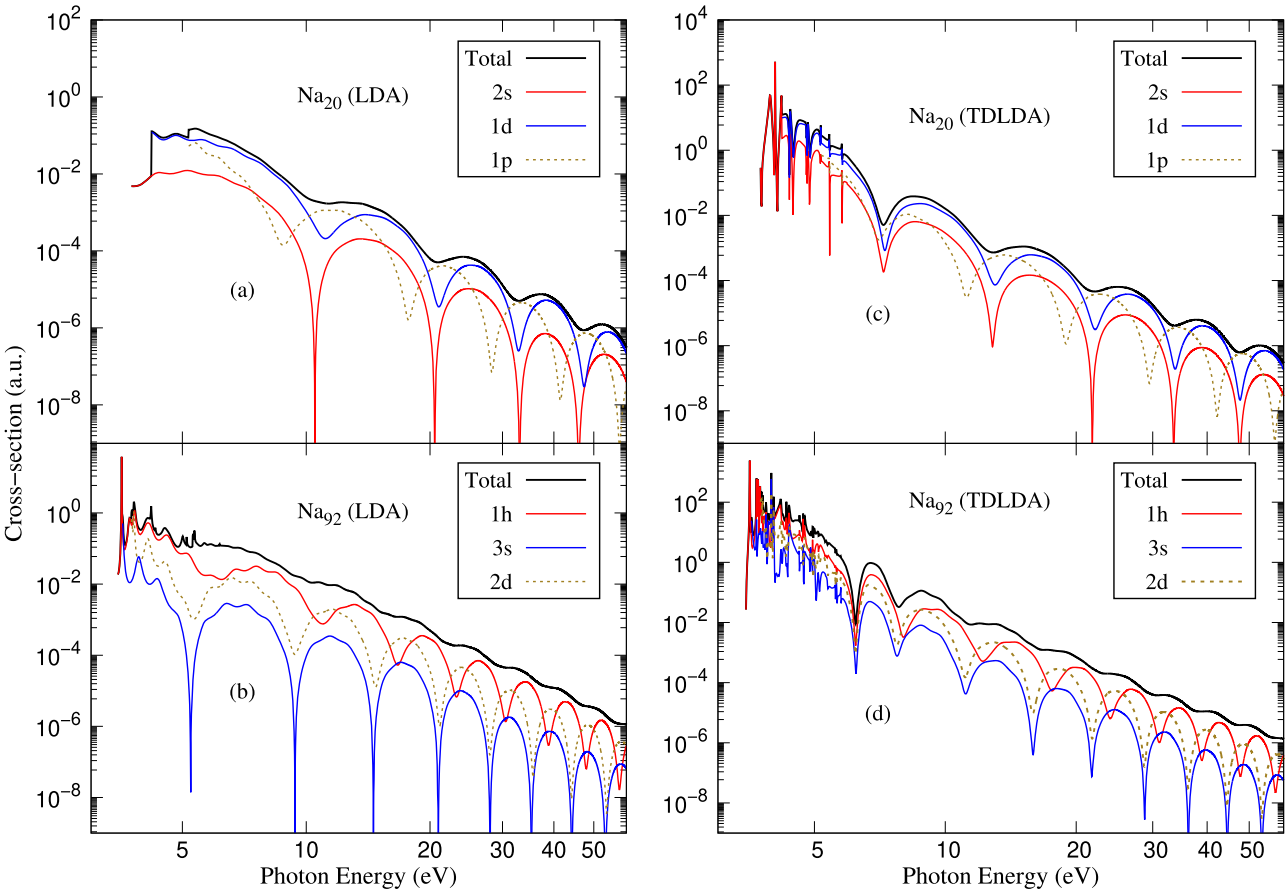

Figure 6. Subshell cross-sections for Na_{20}, (a) and (c), and Na_{92}, (b) and (d), compared with corresponding total cross-section obtained using LDA (left-panels) and TDLDA (right panels).

energies where the plasmon structure begins to fizzle. The oscillations far above the plasmon region are well understood, accessed in experiments [11] and attributed to the diffraction of the photoelectron waves from the edges of the cluster [12]. Since the feature is associated with the cluster geometry, it is seen even in the IP LDA results. The merging of the oscillations at higher energies in TDLDA and LDA reflects on the fact that the higher-energy oscillations are unaffected by the electron correlations. However, the TDLDA cross sections reveal a rather strong minimum occurring at 7.20 eV for Na_{20} and 6.22 eV for Na_{92} which are clearly missing in their LDA counterparts. Incidentally, this feature was also revealed in earlier calculations [9], but was never properly interpreted.

Further insights into this minimum can be harnessed by looking at the individual subshell cross sections. In figure 6 are shown the cross sections from the three outermost subshells of Na_{20} and Na_{92} along with the total cross sections obtained from LDA [figures 6(a) and (b)] and TDLDA [figures 6(c) and (d)]. It is clear in the TDLDA results of each cluster that for all subshells, irrespective of their angular momentum character, this minimum in question occurs dramatically at the same low energy to create a rather emphatic minimum in the total cross section. But such energy-concurrence, independent of subshell angular characters, is totally absent in the LDA curves.

For a subshell, while the creation of a minimum derives directly from the ionization amplitude, its position in energy traces to the ionization phase. The positions of the minima at high energies are seen to be very sensitive to the ionizing subshells. It was shown earlier that the energy-positions of high energy minima are a function of the scattering phase of the individual subshell LDA transition amplitudes [45], since the contribution of $V_{\rm ind}$ in equation (6) is virtually zero at these energies. At very high energies, the contributions to the scattering-phase from even the short-range and Coulomb potentials are negligible. As a result, the final state wavefunction is approximately of the form $\psi_{\rm f} \approx \cos(kr - \frac{\ell'\pi}{2})$, where $\ell' = \ell \pm 1$ in the dipole rule and 'k' is the photoelectron momentum. Further, due to the diffraction of the photoelectrons from the cluster edge, the dominant contribution to the amplitude arises from $r = R_{\rm c}$ which causes the series of minima, the diffraction fringes, seen. Consequently, the squared transition amplitudes differ by a phase of $\Delta\ell'\pi$, which maps to $\Delta\ell\pi$ disregarding the extra 2π phase from $\ell' = \ell \pm 1$. This explains why the oscillations in the cross sections of two subshells of angular momenta differing by an odd integer, such as, s and p, p and d, s and h etc are roughly out-of-phase, while those differing by an even integer, such as, s and d, p and f etc are roughly in-phase. This feature is seen in both LDA and TDLDA subshell results at very high energies. At not-so-high energies, these patterns are not seen to be exactly followed

due to non-negligible short-range and Coulomb phases. The details of the analysis can be found in reference [46]. Note in figure 6 that this ℓ-dependent offset induces a cancellation effect to result in weaker minima in the LDA total cross section at all energies and in the TDLDA total cross section at higher energies.

On the other hand, the energy-concurrent minima in the TDLDA subshell profiles occur at low enough energies and are found 'universal', that is free of any choice of ℓ. Even though the diffraction mechanism forming oscillations still approximately survives, these low energies are in the waning part of the plasmon structure. Hence, the contribution from the correlation phase [42], the phase of the amplitude with some strength of $V_{\rm ind}$, already breaks the pattern from $\ell'\pi$. The correlation phase, being collective in nature, is ℓ-independent, leading to all subshells experiencing practically the same correlation phase. However, there is more in this mechanism. Note that the values of $\mathrm{Re}(V_{\rm ind})$ at the energies [indicated in figure 5] of these minima are sufficiently large and smoothly varying in r. This enables emissions also from a range of r around the cluster edge $r = R_{\rm c}$ due to the access to ionizing force $dV/\mathrm{d}r$. Resulting r-integration weakens the diffraction effect and 'dephases' out the effect of $\ell'\pi$ almost completely. This ensures the minimum for all the subshells to appear coherently at the same energy. Since this coherence originates from a direct onset of correlations via $\mathrm{Re}(V_{\rm ind})$ competing with diffraction, we call this feature the correlation minimum. These minima can, in principle, be probed by the PES or even by the total cross section measurement. At low energies, a faster decrease of the energy-separation between successive minima is noted in TDLDA, in contrast to LDA, as the energy lowers up to the correlation minimum. This trend facilitates the in-phase coherence of this minimum. At even lower energies the collective effect entirely dominates.

4. Conclusions

In summary, the present jellium based linear response DFT calculation describes the remnant of the giant surface and the bulk of the volume plasmon in the photoionization cross section of Na_N ($N = 20$ and 92) clusters. Results show that an appreciable amount of plasmon spillover into the ionization continuum occurs in these systems. The steady background part of the cross section exhibits reasonably good agreement with previous experimental results of the absorption of these clusters. However, a detailed scrutiny of the OS calculated from the cross section and its comparison with the strength extracted from the measurements enables us to quantify the contribution of the single electron Auger-type resonances that the theory predicts. Such, rather narrow, resonances shown in the theory, which does not incorporate the temperature and vibro-rotational effects, are missing in the measurements that include these effects. Furthermore, a deeper scrutiny of the many-body induced self-consistent DFT field reveals the presence of an attractive force in the plasmon spillover energy region. We speculate that this force can cause an observable delay in the emission of photoelectrons at these energies, enabling these clusters as interesting candidates for time-delay measurements. The current study further uncovers the presence of a correlation minimum in the cross sections which appears at the waning range of the plasmon resonance structure. Photoionization measurements of metallic clusters are needed to improve the level of comparisons with current calculations and to test the predictions. Finally, the collective-motion driven spectral properties divulged in this DFT study of Na clusters are likely quite general and may apply at various degrees of prominence in other metallic clusters.

Acknowledgments

The research is supported by the SERB, India, Grant No. EMR/2016/002695 (HRV) and by the US National Science Foundation Grant No. PHY-1806206 (HSC).

Data availability statement

The data that support the findings of this study are available upon reasonable request from the authors.

ORCID iDs

Rasheed Shaik https://orcid.org/0000-0002-0188-8721
Hari R Varma https://orcid.org/0000-0001-9072-0041
Himadri S Chakraborty https://orcid.org/0000-0001-5758-6418

References

[1] Jena P and Sun Q 2018 Super atomic clusters: design rules and potential for building blocks of materials *Chem. Rev.* **118** 5755
[2] Halperin W P 1986 Quantum size effects in metal particles *Rev. Mod. Phys.* **58** 533
[3] Tony S 1988 How small is a solid? *Nature* **331** 116
[4] Castleman A W Jr and Khanna S N 2009 Clusters, superatoms, and building blocks of new materials *J. Phys. Chem.* C **113** 2664
[5] Dinh P M, Reinhard P G and Suraud E 2013 *An Introduction to Cluster Science* (New York: Wiley) pp 127–57
[6] Kreibig U and Vollmer M 2013 *Optical Properties of Metal Clusters* vol 25 (Berlin: Springer)
[7] Xia C, Yin C and Kresin V V 2009 Photoabsorption by volume plasmons in metal nanoclusters *Phys. Rev. Lett.* **102** 156802
[8] Madjet M E-A and Chakraborty H 2009 Collective resonances in the photoresponse of metallic nanoclusters *J. Phys.: Conf. Ser.* **194** 022103
[9] Ekardt W 1985 Size-dependent photoabsorption and photoemission of small metal particles *Phys. Rev.* B **31** 6360
[10] Miroshnichenko A E, Flach S and Kivshar Y S 2010 Fano resonances in nanoscale structures *Rev. Mod. Phys.* **82** 2257
[11] Jänkälä K, Tchaplyguine M, Mikkelä M-H, Björneholm O and Huttula M 2011 Photon energy dependent valence band response of metallic nanoparticles *Phys. Rev. Lett.* **107** 183401
[12] Madjet M E, Chakraborty H S and Rost J-M 2001 Spurious oscillations from local self-interaction correction in high-energy photoionization calculations for metal clusters *J. Phys. B: At. Mol. Opt. Phys.* **34** L345

[13] Bartels C, Hock C, Huwer J, Kuhnen R, Schwöbel J and von Issendorff B 2009 Probing the angular momentum character of the valence orbitals of free sodium nanoclusters *Science* **323** 1323
[14] Mirin N A, Bao K and Nordlander P 2009 Fano resonances in plasmonic nanoparticle aggregates *J. Phys. Chem.* A **113** 4028
[15] Loo C, Lowery A, Halas N, West J and Drezek R 2005 Immunotargeted nanoshells for integrated cancer imaging and therapy *Nano Lett.* **5** 709
[16] Liao H, Nehl C L and Hafner J H 2006 Biomedical applications of plasmon resonant metal nanoparticles *Nanomedicine* **1** 201
[17] Ferrell R A 1958 Predicted radiation of plasma oscillations in metal films *Phys. Rev.* **111** 1214
[18] Onida G, Reining L and Rubio A 2002 Electronic excitations: density-functional versus many-body Green's-function approaches *Rev. Mod. Phys.* **74** 601
[19] Choi J, Chang E, Anstine D M, Madjet M E and Chakraborty H S 2017 Effects of exchange–correlation potentials on the density-functional description of C_{60} versus C_{240} photoionization *Phys. Rev.* A **95** 023404
[20] Shaik R, Varma H R and Chakraborty H S 2020 Effects of exchange–correlation functionals on the structure and the photoionization dynamics of Na_{40} versus Na_{92} cluster *J. Phys.: Conf. Ser.* **1412** 102009
[21] Chandezon F, Bjørnholm S, Borggreen J and Hansen K 1997 Electronic shell energies and deformations in large sodium clusters from evaporation spectra *Phys. Rev.* B **55** 5485
[22] Van Leeuwen R and Baerends E J 1994 Exchange–correlation potential with correct asymptotic behavior *Phys. Rev.* A **49** 2421
[23] Oliver G L and Perdew J P 1979 Spin-density gradient expansion for the kinetic energy *Phys. Rev.* A **20** 397
[24] Madjet M E, Chakraborty H S, Rost J M and Manson S T 2008 Photoionization of C_{60}: a model study *J. Phys. B: At. Mol. Opt. Phys.* **41** 105101
[25] Petersilka M, Gossmann U J and Gross E K U 1996 Excitation energies from time-dependent density-functional theory *Phys. Rev. Lett.* **76** 1212
[26] Feibelman P J 1975 Microscopic calculation of electromagnetic fields in refraction at a jellium–vacuum interface *Phys. Rev.* B **12** 1319
[27] Bertsch G 1990 An RPA program for jellium spheres *Comput. Phys. Commun.* **60** 247
[28] Fano U 1961 Effects of configuration interaction on intensities and phase shifts *Phys. Rev.* **124** 1866
[29] Javani M H, Wise J B, De R, Madjet M E, Manson S T and Chakraborty H S 2014 Resonant Auger–intersite-Coulombic hybridized decay in the photoionization of endohedral fullerenes *Phys. Rev.* A **89** 063420
[30] De R, Magrakvelidze M, Madjet M E, Manson S T and Chakraborty H S 2016 First prediction of inter-Coulombic decay of C_{60} inner vacancies through the continuum of confined atoms *J. Phys. B: At. Mol. Opt. Phys.* **49** 11LT01
[31] Bertsch G F and Tománek D 1989 Thermal line broadening in small metal clusters *Phys. Rev.* B **40** 2749
[32] Penzar Z, Ekardt W and Rubio A 1990 Temperature effects on the optical absorption of jellium clusters *Phys. Rev.* B **42** 5040
[33] Solov'yov A V, Polozkov R G and Ivanov V K 2010 Angle-resolved photoelectron spectra of metal cluster anions within a many-body-theory approach *Phys. Rev.* A **81** 021202
[34] Polozkov R G, Ivanov V K, Verkhovtsev A V, Korol A V and Solov'yov A V 2013 New applications of the jellium model for the study of atomic clusters *J. Phys.: Conf. Ser.* **438** 012009
[35] Magrakvelidze M, Anstine D M, Dixit G, Madjet M E and Chakraborty H S 2015 Attosecond structures from the molecular cavity in fullerene photoemission time delay *Phys. Rev.* A **91** 053407
[36] Trabattoni A *et al* 2019 Real-time probing of the plasmonic response of C_{60} *7th Int. Conf. on Attosecond Science and Technology* (Budapest, Hungary) (University of Szeged Congress Centre) pp 1–5
[37] Cheng C-H *et al* 2019 Photoinduced ultrafast electron transfer and charge transport in a PbI_2/C_{60} heterojunction *J. Phys. Chem.* C **123** 30791
[38] Ali E, Madjet M E and Chakraborty H S 2021 Vibrational relaxation of photoexcited electrons in fullerenes *51st Annual Meeting of the APS Division of Atomic, Molecular and Optical Physics* volume 65 (Portland, Oregon) Number 4Bulletin of the American Physical Society
[39] Wendin G 1973 Collective effects in atomic photoabsorption spectra. III. Collective resonance in the 4d 10 shell in Xe *J. Phys. B: At. Mol. Phys.* **6** 42
[40] Zangwill A and Soven P 1980 Density-functional approach to local-field effects in finite systems: photoabsorption in the rare gases *Phys. Rev.* A **21** 1561
[41] Schultze M *et al* 2010 Delay in photoemission *Science* **328** 1658
[42] Magrakvelidze M, Madjet M E, Dixit G, Ivanov M and Chakraborty H S 2015 Attosecond time delay in valence photoionization and photorecombination of argon: a time-dependent local-density-approximation study *Phys. Rev.* A **91** 063415
[43] Pazourek R, Nagele S and Burgdörfer J 2015 Attosecond chronoscopy of photoemission *Rev. Mod. Phys.* **87** 765–802
[44] Magrakvelidze M, Madjet M E and Chakraborty H S 2020 Correlation drives a strong attractive force on plasmonic photoelectrons *J. Phys.: Conf. Ser.* **1412** 072040
[45] Frank O and Rost J-M 1997 *Chem. Phys. Lett.* **271** 367
[46] McCune M A, Madjet M E and Chakraborty H S 2008 Unique role of orbital angular momentum in subshell-resolved photoionization of C_{60} *J. Phys. B: At. Mol. Opt. Phys.* **41** 201003